RESPONSE OF CO$_2$ FLUXES TO THE OCEAN-ATMOSPHERE INTERACTION PROCESSES IN THE FERNANDO DE NORONHA ISLAND

Luis Henrique B. Alves[1]*; Manuel Flores Montes[1]; Nathalie Lefèvre[2]; Thiago Luiz do Vale Silva[3]; Francis Lopes[1]; Doris Veleda[1]

[1] Department of Oceanography – DOCEAN, Federal University of Pernambuco – UFPE, Av. Arquitetura, s/n, Cidade Universitária, 50740-550 Recife, PE, Brazil.

[2] IRD-LOCEAN, Sorbonne Université, 4 place Jussieu, 75252 Paris Cedex 05, France

[3] Pernambuco Water and Climate Agency (APAC), Recife, Brazil

* Corresponding author: luis.alves@ufpe.br

Resumo

Este estudo investiga as condições termodinâmicas e os fluxos ar-mar de CO$_2$ na região da Ilha de Fernando de Noronha. As análises foram baseadas nos resultados de modelagem acoplada oceano-atmosfera para três períodos de cruzeiros oceanográficos, Camadas Finas I, Camadas Finas II e Camadas Finas IV, em 2010, 2012 e 2014. Os resultados da modelagem oceano-atmosfera correspondem bem aos dados dos três cruzeiros oceanográficos ao redor da ilha. O vento modelado teve boa correlação com os valores de velocidade e direção do vento em 10m, com significância estatística de 95%. A temperatura da superfície do mar e as correntes superficiais são modificados com a presença da ilha. No lado oeste da ilha, as correntes oceânicas são enfraquecidas devido à barreira física e a temperatura da superfície do mar aumenta, indicando um efeito ilha. O efeito ilha também é observado ao analisar as seções verticais. As condições meteorológicas em 2010 mostram que a temperatura do ar foi mais elevada do que em 2012 e 2014. A atmosfera também apresenta um efeito de ilha, com o vento contornando o terreno superior da ilha e enfraquecendo a sotavento. A parte oceânica mostra um aquecimento das águas superiores e convergência de correntes no lado oeste da ilha. As temperaturas oceânicas modeladas subestimam ($\sim$ -0,3 °C) as observações, exceto a oeste da ilha ($\sim$ +0,3 °C), onde a temperatura do modelo é superior às medidas. O cálculo do viés de FCO$_2$ (fCO$_2$ é a fugacidade de CO$_2$ com unidade μatm, FCO$_2$ é o fluxo de CO$_2$) mostra que o modelo subestima as medições em cerca de 20 mmol m^{-2} d^{-1}. O oceano foi fonte de CO$_2$ durante os três períodos de cruzeiro oceanográfico.

Palavras-Chave: Fernando de Noronha, efeito ilha, fluxos de CO$_2$ oceano-atmosfera.

Abstract

This study investigates thermodynamic conditions and air-sea CO$_2$ fluxes in the Fernando de Noronha Island region. The analyses were based on coupled ocean-atmosphere modeling results for three periods of oceanographic cruises, Camadas Finas I, Camadas Finas II, and Camadas Finas IV, in 2010, 2012, and 2014. The ocean-atmosphere modeling results correspond well with data from three oceanographic cruises around the island. The modeled wind correlated well with the wind speed and direction values at 10m, with a statistical significance of 95%. The presence of the island modifies the sea surface temperature and surface currents. On the island's west side, ocean currents are weakened due to the physical barrier, and the sea surface temperature increases, indicating an island effect. The island effect is also observed when analyzing vertical sections. Weather conditions in 2010 show that the air temperature was higher than in 2012 and 2014. The atmosphere also exhibits an island effect, with the wind skirting the island's upper terrain and weakening on the leeward side. The oceanic part shows the warming of the upper waters and the convergence of currents on the island's west side. Modeled ocean temperatures underestimate ($\sim$ -0.3 °C)

observations, except to the west of the island ($\sim$ +0.3 °C), where model temperatures are higher than measurements. Calculation of the FCO2 bias (fCO$_2$ is the CO$_2$ fugacity with unit atm, and FCO$_2$ is the CO$_2$ flux) shows that the model underestimates the measurements by about 20 mmol m^{-2} d^{-1}. The ocean was a source of CO$_2$ during the three oceanographic cruise periods.

Keywords: Fernando de Noronha, island effect, ocean-atmosphere CO$_2$ fluxes

Introduction

The western tropical Atlantic (WTA) is characterized by strong thermal stratification and permanent thermocline, with oligotrophic waters, low concentration of nutrients, and planktonic biomass. However, islands and seamounts can trigger mechanisms that change the local hydrodynamics, affecting the surrounding circulation, causing vertical mixing, and favoring productivity. This phenomenon is called the "island effect" (Gove et al., 2016). Araujo and Cintra (2009) also point out that the interaction of currents with the topography of islands and seamounts can lead to the production of eddies, currents weakening, and disturbances in the thermohaline structure. The Fernando de Noronha (FN) Archipelago is in WTA and is under the influence of the central branch of the South Equatorial Current (cSEC) in the upper layer. This zonal current flows westward to join the North Brazil Undercurrent (NBUC) along the Brazilian coast. Measurements of the cSEC at 3-7°S and 30°W show an average intensity of 0.34m s^{-1}, with a seasonal variability expressed by a bimodal decrease until early April and November and strengthening in mid-July (Lumpkin and Garzoli, 2005). Below the cSEC, between 2.5 - 4° S, the southern branch of the Equatorial Undercurrent (SEUC) in the 200-500 m depth flows eastward.

FN has been subject to numerous biological studies (Brandão et al., 2017; Garla et al., 2006; Leite et al., 2009; Vargas et al., 2018). However, the island's interaction with the current systems and its consequences on the local marine ecosystem is still poorly known. The presence of the FN generates changes in ocean circulation, temperature, and salinity (Tchamabi et al., 2017). Recently, Costa da Silva et al. (2021) identified that flow-topography induced changes in the thermohaline structure and biogeochemistry in the southeast of the island, presenting negative temperature and salinity anomalies between 200 and 400 m and fluorescence peak. The development of eddies and turbulence usually occur in areas of islands, increasing primary production and sinking the amount of atmospheric CO$_2$ to the ocean. Otherwise, other features generated by islands, such as warm wakes at the surface, increase the sea surface temperature (SST), which is frequently found in the lee of islands (Pullen et al., 2017; Sangrà et al., 2007; Caldeira et al., 2002).

Using a regional ocean model, Tchamabi et al. (2017) simulated the thermodynamics and surface circulation in the oceanic region of FN and Atol das Rocas (AR). These authors identified a weakening of the surface current (cSEC) downstream of the islands. A small-scale cooling was detected at 60m depth west of the island. This subsurface cooling, primarily driven by the disruption of the cSEC by the bathymetry of the island, results from the action of eddies downstream FN through turbulent mixing. However, these authors focus mainly on the subsurface effects and neglect the upper ocean temperature wakes.

Warm SSTs are commonly found on the leeward of islands (Caldeira et al., 2002). Caldeira and Tomé (2013) hypothesized that atmospheric wakes' cloud-free conditions promote enhanced short-wave radiation and lee-side ocean warming. Caldeira and Marchesiello (2002) found 4–5°C above the surrounding upper oceanic waters, downwind of islands in the first 20m depth. Caldeira et al. (2002) also detected 2–3°C warmer surface waters at leeward of Madeira in the first 20m. Han et al. (2019) found the mean SST west of Madagascar Island up to about 3.0 °C warmer than in the east. The presence of Madagascar Island resulted in weaker winds on the leeward side and, in turn, weakened the mixing in the upper waters; thus, a shallower surface mixed layer depth.

Consequently, small SST changes in these warm waters may strongly impact air-sea fluxes and lead to changes in carbon budget estimates. It is necessary to understand better the role of the ocean islands in biogeochemical cycles and feedback. Thus, observations and models improve our understanding of the coastal zone concerning the carbon budget.

Chaves et al. (2006) showed that primary production rises in adjacent Fernando de Noronha Island areas. Several studies suggested that high productivity is linked to upwelling due to the island's topography (Ekau & Knoppers, 1999; Silva et al., 2019; Araujo et al., 2019). Caldeira et al. (2005) investigated the island mass effect in Southern California Bight under the wind and current dynamics. Moreover, they noted that this effect affects the island's primary productivity. Bakker et al. (2007) quantified the island mass effect for inorganic carbon changes and CO_2 air-sea fluxes in the Crozet Plateau waters. These authors identified phytoplankton blooms downstream of the plateau, creating an oceanic CO_2 sink.

Air-sea CO_2 fluxes (FCO_2) in many coastal systems are often based on snapshot measurements. Thus, spatial and temporal changes in FCO_2 remain to be resolved, as significant uncertainties are often reported in individual systems, which would, in turn, impact the estimation of global fluxes. From the

perspective of predictability of future changes, air-sea FCO_2 space-time variability and the inherent controlling processes need to be better understood (Zhai et al., 2013).

Studies in other regions showed that FCO_2 changes over the year (Burgers et al., 2017; Bates et al., 2011; Drupp et al., 2011; Dumousseaud et al., 2010) and that coral reefs could be a CO_2 source to the atmosphere (Yan et al., 2011; Ware et al., 1992). Torres et al. (2020) evaluated the sensitivity of CO_2 air-sea gas exchange in a coastal station in the western English Channel. They performed four different model system configurations of the 1D coupled hydrodynamic–ecosystem model GOTM–ERSEM towards identifying critical dynamics of relevance in quantifying air-sea CO_2. These authors found that numerical experiments resolving near-surface temperature gradients induced by the daily heating cycle have the most efficient impact at short, seasonal, and annual time scales.

Long-term air-sea CO_2 fluxes have been difficult to quantify due to the lack of field data measurements (Schuster et al., 2009; Fransson et al., 2008; Padin et al., 2010; Dumousseaud et al., 2010; Dai et al., 2009). Hence, continuous spatial monitoring efforts are required to assess the air-sea CO_2 variability with a level of reliability. Space-time observations are limited in open ocean areas. Models are an alternative to supply spatial estimative about the variability of these fluxes around islands, which can be achieved using an ocean-atmosphere coupled model (Arístegui et al., 1997). Hence, this paper aims to quantify the air-sea CO_2 fluxes around Fernando de Noronha Island using a coupled ocean-atmosphere high-resolution model, in situ physical variables, and seawater CO_2 fugacity.

Methods

Study area

The Fernando de Noronha Archipelago (FN) (03 ° 45'-03 ° 57 'S, 32 ° 19'-32 ° 41' W) (Figure 1) is located 345 km from the Brazilian coast and consists of 21 islands, islets, and rocks, covering an area of 18.4 km². The main island, Fernando de Noronha Island, constitutes 91% of the archipelago's total area. It is the largest archipelago in Brazil and includes a National Marine Park and a State Environmental Protection Area under the jurisdiction of the ICMBio - Chico Mendes Institute for Biodiversity Conservation. The dynamic of the winds is linked to the seasonal migration of the Intertropical Convergence Zone (ITCZ). The ITCZ is centered in the zone of maximum SSTs in the equatorial region, migrating in boreal winter to its southernmost position

when the island is under the influence of the northeast trade winds. In boreal summer and autumn, the ITCZ is at its northernmost part, and the southeasterly winds prevail.

The FN region is characterized by a rainy season between March and July and a dry season between August and January (Mohr et al., 2009). The tidal regime is semi-diurnal, with an amplitude of 2-3.2 m (Mohr et al., 2009). The archipelago is directly influenced by the central branch of the South Equatorial Current (cCSE), with an average salinity of 36 and temperatures between 26 and 28°C (Costa da Silva et al., 2021).
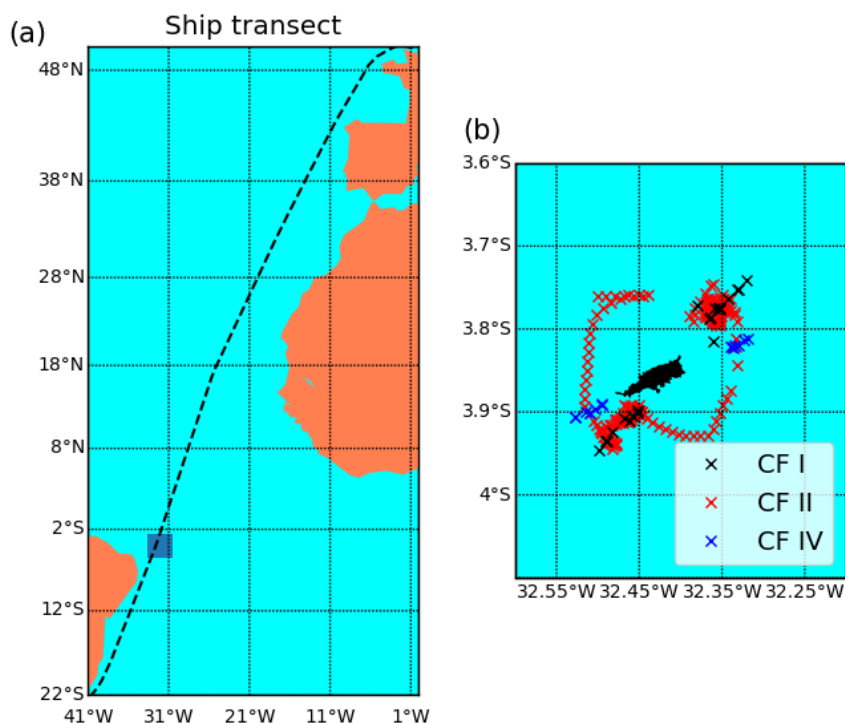
Figure 1. (a) Fernando de Noronha Island. (b) Fernando de Noronha Island geographic position and contour with CF I, CF II and IV CTD's samples.

Air-sea coupled modeling

Here, we used a coupled model composed of the Regional Ocean Modeling System (ROMS) (Shchepetkin and McWilliams, 2005) and Weather Research and Forecasting (WRF) model (Skamarock et al., 2008) as the oceanic and atmospheric components, respectively. The models were coupled using the Model Coupling Toolkit (MCT) (Jacob et al., 2005; Larson et al., 2005). The implementation occurred through the COAWST (Warner et al., 2010). The ROMS model is a three-dimensional, free-surface, terrain-flowing numerical model that solves the Reynolds-averaged Navier-Stokes equations using the hydrostatic and Boussinesq assumptions

(Shchepetkin & McWilliams, 2005) . ROMS has been specially designed for accurate regional marine systems simulations for various applications (Warner et al., 2005; Wilkin et al., 2005) .

The atmospheric model component in COAWST is the compressible and non-hydrostatic model WRF (Skamarock et al., 2008) . The WRF has different schemes for representing the physics of the atmospheric boundary layer and physical parameterization of processes on a subclass scale.

The Model Coupling Toolkit (MCT) is a coupler in the COAWST modeling system for different model components (Jacob et al., 2005; Larson et al., 2005) . The coupler uses a parallel coupling approach to facilitate the transference and transformation of various component models' parameters—the MCT coupler exchanges prognostic variables from one model component to another. The WRF model receives SST from the ROMS and supplies the zonal and meridional wind components at 10 m, atmospheric pressure, relative humidity, cloud fraction, rainfall, and short and longwave radiation to the ROMS model (Warner et al., 2010) .

The coupled model was configured for a domain covering the Fernando de Noronha area from July 10 to August 06, 2010, and July 1 to August 31, 2014. The COAWST configuration used in this study included the coupled atmosphere-ocean model (ROMS + WRF) but did not include the wave and sediment transport models. The WRF is a non-hydrostatic atmospheric model, fully compressible with a vertical terrain coordinate system. The WRF model was configured with two nested domains, the first one with 9 km horizontal degree resolution covering the area 25° - 38 ° W, 10° S - 2° N, the second one with 3 km restricted to 30° to 34 ° W, 5° - 2° S and 42 vertical sigma coordinates. The WRF initial and lateral boundary conditions are from the Final Analysis (FNL) of the National Environmental Prediction Centers (NCEP) (NCEP FNL, 2000), with an interval of 6 hours. WRF was configured following Table (1).

Table 1 - WRF Model Namelist Settings

Grid Structure	Arakawa C-grid
Time step for integration	60 seconds
Microphysics scheme	WRF Single–moment 6–class Scheme
Longwave and Shortwave radiation scheme	RRTMG Shortwave and Longwave Schemes
Surface Layer	NCEP Global Forecast System Scheme
Boundary layer scheme	Mellor–Yamada Nakanishi Niino (MYNN) Level 2.5 and Level 3 Schemes
Cumulus parameterization scheme	Kain–Fritsch Scheme

The terrain-following ocean model ROMS has one domain with a horizontal grid resolution of 1 km (Figure 1) in the 31°13' W – 33°36' W and 2°37' S – 5° S. This high resolution in ROMS allows us to solve mesoscale eddies in the ocean. Initial and lateral open boundary conditions were derived from HYCOM (Wallcraft et al., 2009), with a horizontal resolution of 0.08◦x0.08◦. The

bathymetry data for the simulations were taken from the GEBCO, a global continuous terrain model for ocean and land with a spatial resolution of 15 arc seconds (GEBCO, 2021). The grid uses Version 2.2 of the SRTM15 plus data set (Tozer B. et al., 2019). The main parameterizations used in ROMS are available in Table (2).

Table 2 - ROMS Standard Input Parameters

Grid Structure	Arakawa C-grid
Time step for integration	10
Number of barotropic time steps	40
Thermal expansion coefficient	1.7×10^{-4}
Linear bottom drag coefficient	3×10^{-4} m/s
Mean density for Boussinesq approximation	1025 kg/m^3
Lateral boundary layer	Free surface: Chapman implicit (free surface)
	Baroclinic currents: Flather (2D momentum)
	Barotropic currents: Radiation + Nudging
	Tracers: Radiation + Nudging
S-coordinate bottom control parameter	0.1
Vertical transform equation	2
Vertical stretching function	2

CTD, satellite and wind measurements

Temperature and salinity from Conductivity-Temperature-Depth measures (CTDs) profiles of the oceanographic cruises, Camadas Finas I in August 2010 (CF2010), Camadas Finas II in September 2012 (CF2012), and Camadas Finas IV in July 2014 (CF2014), were used to compare with the ocean model results. The validation of all profiles was carried out from the surface to 300 meters depth for the following 14 depths: 16.505, 22.465, 29.841, 38.870, 49.796, 62.867, 78.340, 96.480, 117.556, 141.843, 169.622, 201.172, 236.767 and 276.664 meters.

The profiles of the modeled variables were organized simultaneously, with every point corresponding to a respective depth of the CTD data. The correlation and standard deviation between the simulated and observed temperature and salinity were calculated for each profile using the Taylor diagram (Taylor, 2001).

The SST and SSS satellite data were compared with the model results. Satellite SST is from MODIS Aqua, 8-day night average, 11µm, with 4km resolution. The SSS is from MIRAS SMOS, with 0.25 degrees of spatial resolution, https://earth.esa.int/eogateway/instruments/miras.

Wind data compared with model wind results are from a local meteorological station, number 32564, available by the Center for Weather Forecasting and Climate Studies of the National Institute for Space Research (CPTEC/INPE), https://www.cptec.inpe.br/.

The seawater CO_2 fugacity (fCO_2sw) measurements from CF2012 were used to validate the fCO_2sw estimative from modeled variables.

Air-sea CO$_2$ flux estimative

To calculate the air-sea FCO_2, we used the oceanic and atmospheric variables from the atmospheric-ocean coupled model COAWST, as the SST (K), SSS, surface winds (m s^{-1}) and the sea level pressure (atm). The atmospheric CO_2 fugacity (fCO_2atm) is calculated from the CO_2 molar fraction, from the World Data Centre for Greenhouse Gases (WDCGG), operating in the Japan Meteorological Agency.

The difference in partial pressure of CO_2 between the water and air mainly controls the fluxes across the air-sea interface. The FCO_2 (Equation 1) is calculated using a relation between CO_2 solubility, gas exchange coefficient (k) (Equation 3), and the difference of CO_2 fugacity between the ocean and the atmosphere (ΔfCO_2) (Equation 2) (Sweeney et al., 2007; Weiss, 1974; Currie et al., 2011).

$$FCO_2 = k \times \text{Solubility (T, S)} \times \Delta fCO_2 \tag{1}$$

where the Δf CO_2 is given by:

$$\Delta fCO_2 = fCO_{2sw} - fCO_{2atm} \tag{2}$$

and the gas exchange coefficient is given by:

$$k = 0.27 \times U^2 \times (600/Sc)^{0.5} \tag{3}$$

where U is the wind velocity and Sc is the Schmidt number. The Schmidt number is a relation between constants with the temperature of seawater and salinity (Equation 4) (Esters et al., 2017).

$$Sc = 2073.1 - 125.62 \times SST + 3.6276 \times SST^2 - 0.043219 \times SST^3 \tag{4}$$

The sign of the fCO_2 gradient defines the direction of the FCO_2 into the ocean (negative) or to the atmosphere (positive). The estimated fCO_2sw through modeled data is compared with those measured by the CFII 2012 around FN Island.

Lefèvre et al. (2010) propose a relationship between salinity and carbon parameters for the western Tropical Atlantic. In this work, we applied linear regression for fCO_2sw, using salinity and temperature (R2 0.956, N=403). As a result of the local conditions, a regression equation could be determined:

$$fCO_2sw = 92.5325 * SSS - 13.7247 * SST - 2575 \qquad (5)$$

Results and discussion

Model validation

The ability of the model to accurately simulate the hydro-thermodynamical conditions in the influence area of FN is crucial to the quality of the air-sea FCO_2 results. To assess the performance of the COAWST simulation results, we compare them with the CTD measurements, surface winds, and satellite data. The Taylor diagram was applied to each in situ temperature and salinity profile and modeled data. The temperature and salinity profiles from the model were selected in the same geographic coordinates and time of the ship track. Then, both data were compared, applying the sample data as a reference. The correlation for the temperature profile is between 0.84 to 0.99 (Figure 2a,c,e). The salinity correlation is between 0.71 to 0.99 (Figure 2b,d,f). The Taylor diagram shows that the modeled temperature and salinity agree with the thermodynamics around the island.
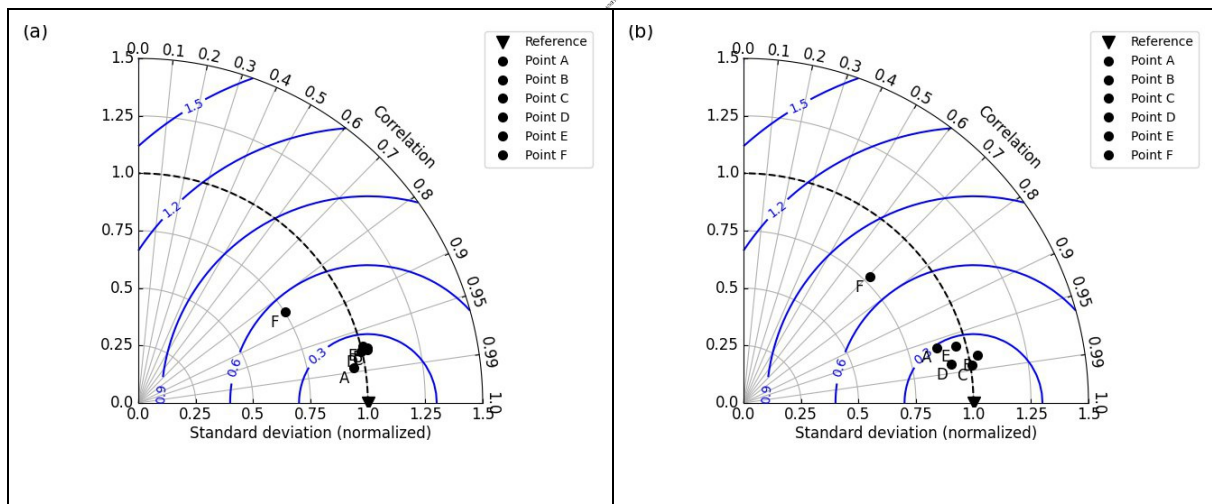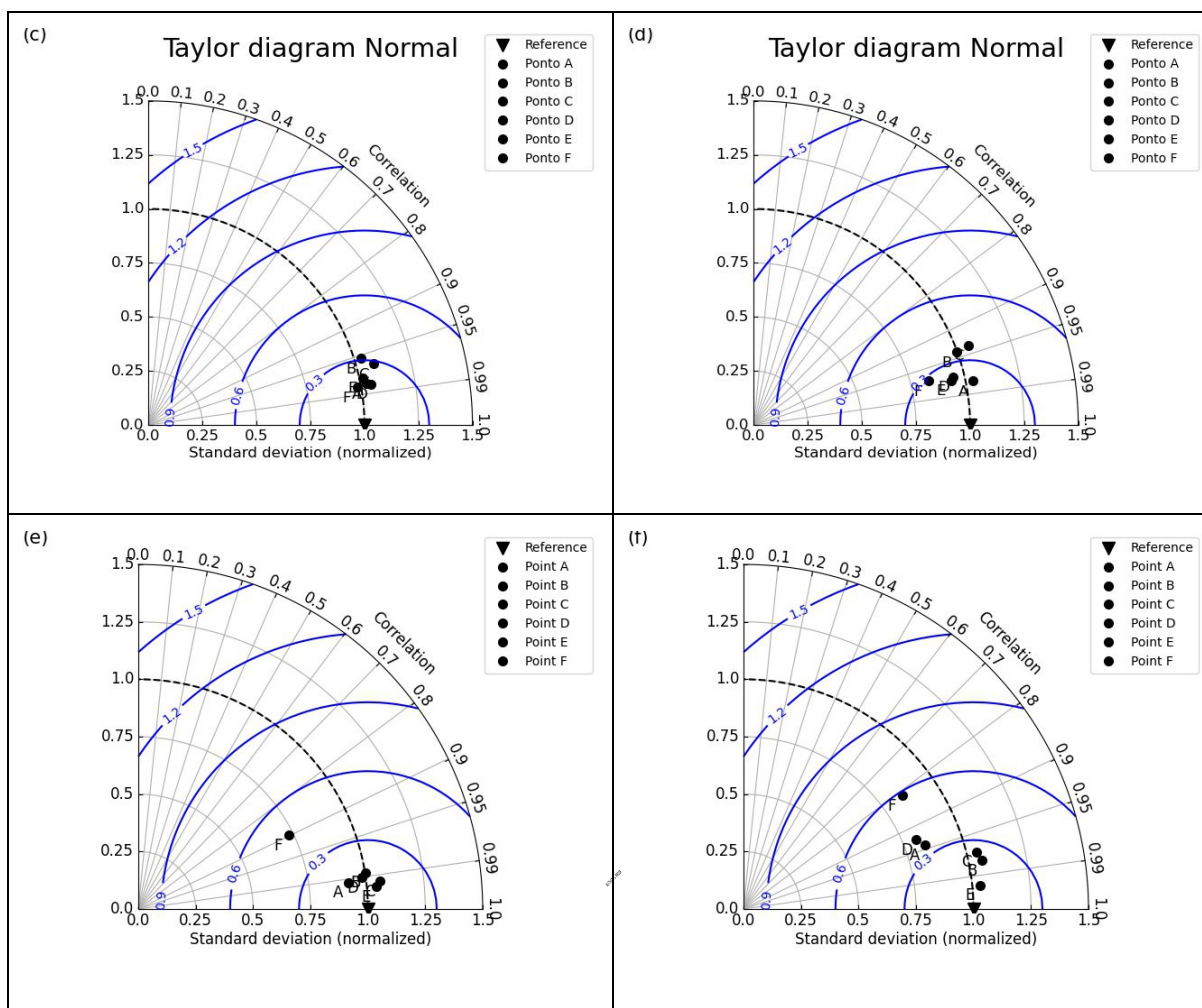
Figure 2. The Taylor diagram between CTD's samples and the model results for: (a) August 2010 simulated and observed temperature, (b) August 2010 simulated and observed salinity, (c) September 2012 simulated and observed temperature, (d) September 2012 simulated and observed salinity, (e) July 2014 simulated and observed temperature and, (f) July 2014 simulated and observed salinity.

Both model results and in situ data are paired in the same length using as criteria: depth, geographic location, and time. Points of CF2010: A (-3.924, -32.483), B (-3.946, -32.499), C (-3.946, -32.499), D (-3.787, -32.365), E (-3.753, -32.332), F (-3.771, -32.379). Points of CF2012: A (-3.934, -32.488), B (-3.910, -32.456), C (-3.911, -32.464), (d) D (-3.761, -32.330), E (-3.764, -32.341), F (-3.772, -32.356). Points of CF2014: A (3.8908°S, 32.4952°W), B (3.8961°S, 32.5020°W), C (3.9016°S, 32.5098°W), D (3.8998°S, 32.5098°W), E (3.9066°S, 32.5270°W), F (3.8218°S, 32.3383°W).

The spatial bias at the surface was performed for SST and SSS between modeled and satellite data. The modeled SST during the day and night (supplemental material) presents a warm bias of 0.5 to 0.6°C compared to the MODIS Aqua SSTs. This result can be associated with the lower resolution of SST satellite data (~4km), while the ROMS modeling is with 1km, which

improves the physical processes near the surface. The modeled SSS presents a bias of 0.1 in the central area of the domain (supplemental material). In this case, the MIRAS SMOS SSS has a resolution of 0.25km, much lower than the model resolution. The ROMS output profiles of temperature and salinity were compared at the same stations and times as the CTD measurements of CF2010 (Figure 3). The model results of temperature profiles show a good adjustment with the in-situ data, mainly in the first 100m depth. The modeled thermocline is less stratified than the observations. The simulations underestimate the salinity profiles, with a difference of about 0.3-0.4psu, mainly at the surface. Figure 4 shows the vertical profiles of temperature and salinity for 2012, and Figure 5 shows for 2014. The model results of temperature and salinity profiles show good agreement with the in-situ data.
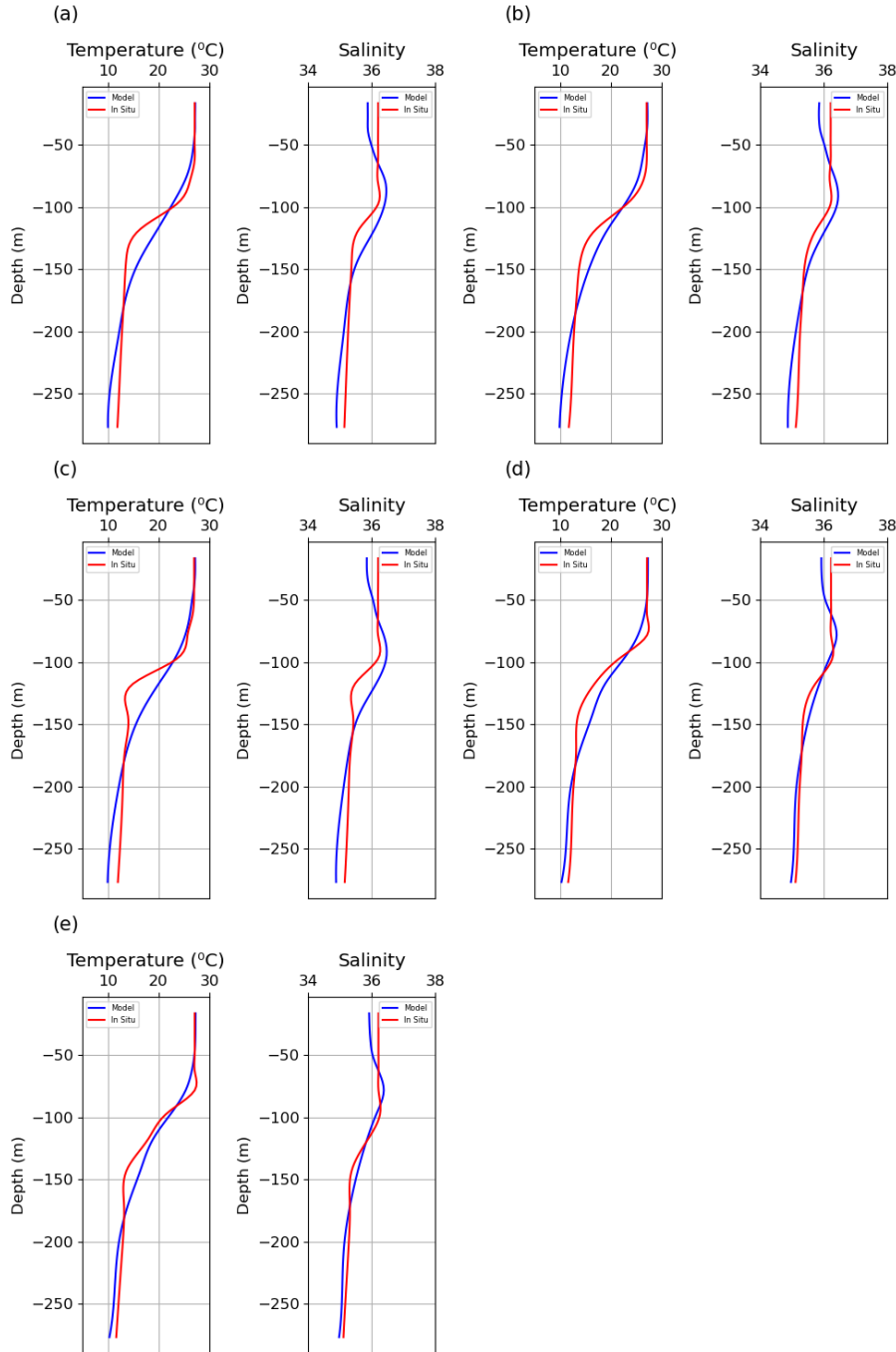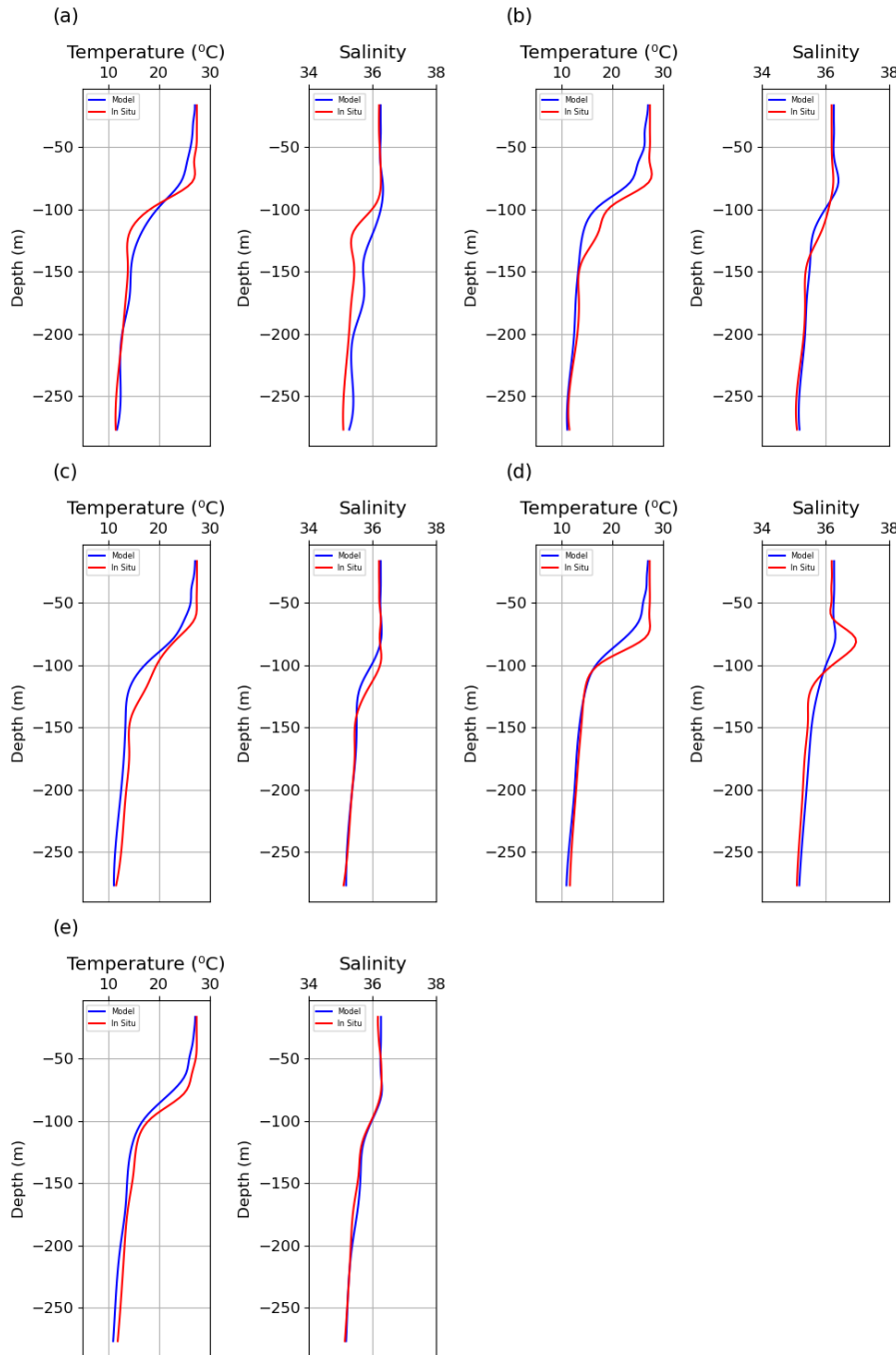
Figure 3. Vertical profiles of temperature and salinity, corresponding to ROMS model and CTD measurements of the CF2010 cruise. The points are: (a) 02 August 2010 21h (-3.924, -32.483), (b) 03 August 2010 04:30h (-3.946, -32.499), (c) 03 August 2010 09:30h (-3.946, -32.499), (d) 01 August 2010 02:30h (-3.787, -32.365), (e) 01 August 2010 10:00h (-3.753, -32.332).
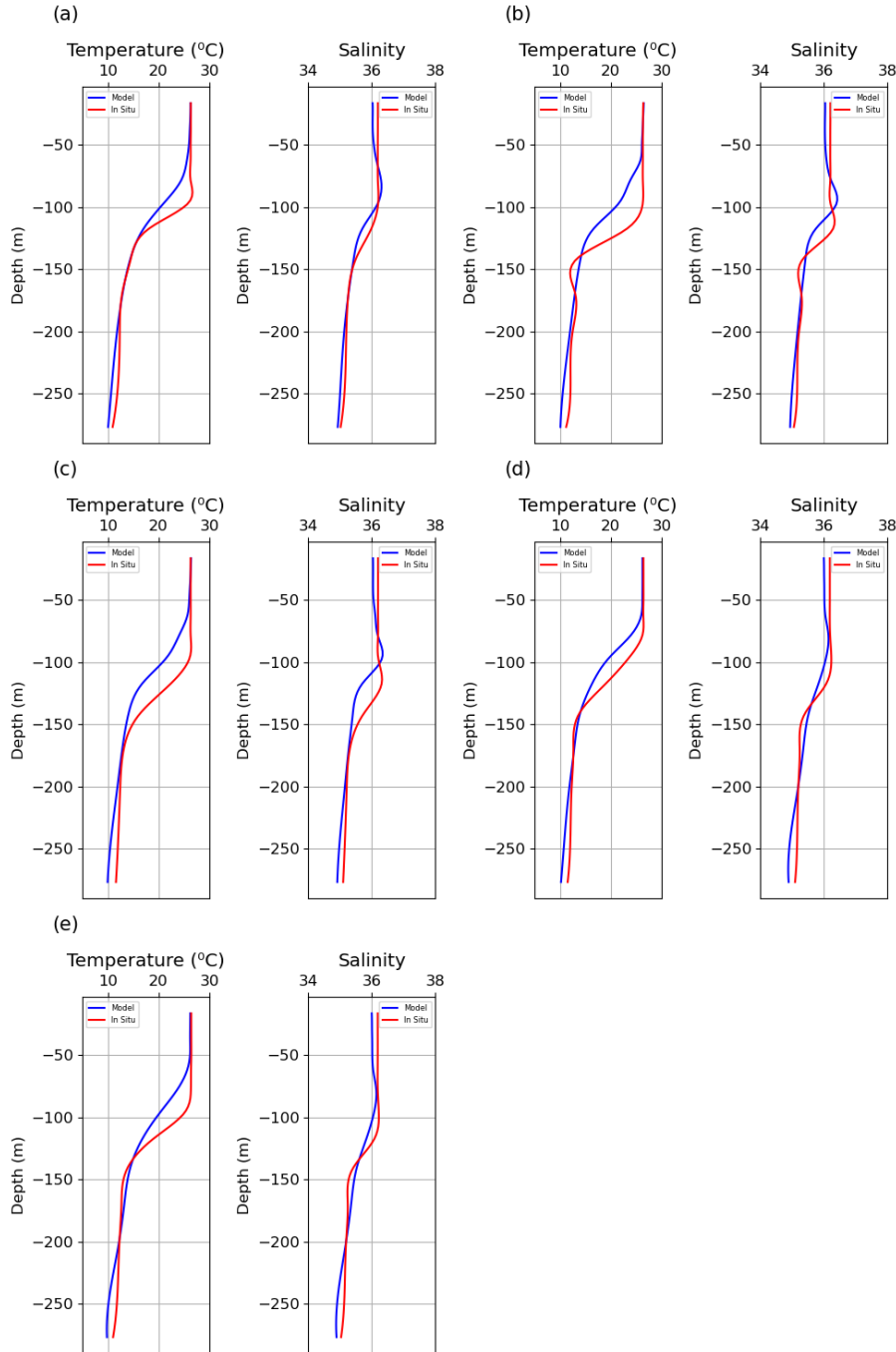
Figure 4. Vertical profiles of temperature and salinity comparisons, corresponding to ROMS model and CTD measurements of the CF2012 cruise. The points are: (a) 24 September 2012 20h (-3.934, -32.488), (b) 25 September 2012 14:19h (-3.910, -32.456), (c) 25 September 2012 03:55h (-3.911, -32.464), (d) 27 September 2012 03h (-3.761, -32.330), (e) 27 September 2012 00:44h (-3.764, -32.341).

Figure 5. Vertical profiles of temperature and salinity comparisons, corresponding to ROMS model and CTD measurements of the CF2014 cruise. The points are: (a) (3.8908°S, 32.4952°W), (b) (3.8961°S, 32.5020°W), (c) (3.9016°S, 32.5098°W), (d) (3.8998°S, 32.5098°W), (e) (3.9066°S, 32.5270°W.

The main speed and direction of observed winds were compared with the model results for the CF2010 and CF2014 periods (supplemental material), except in 2012, when wind measurements were unavailable. The observed winds for 1-3 August 2010 were predominantly

from the southeast, ranging from 9 to 12m/s. On 7-8 July 2014, the winds presented higher variability, changing from 2 to 14m/s, and directions also mainly from the southeast, but with a larger distribution, also showing an east component. The modeled results for 2010 agree with the measurements, with values between 9 and 12m/s, mainly from the southeast. The modeled winds present higher variability for 2014, ranging from 4 to 13m/s, and directions from southeast and east, in agreement with the in-situ data for this period. The wind speed time series 2010 correlates 0,9 (p-value < 0,5) with in situ data from Fernando de Noronha Meteorological Station. The time series from 2014 correlates 0,5 (p-value < 0,5).

Physical parameter analyses

Figures 6, 7, and 8 show the modeled SSTs and surface currents for the same days of the CF2010, CF2012, and CF2014 cruises at 06 AM and 6 PM. During CF2010 (Figure 6), the surface circulation was predominantly from the southeast and weakened downstream of the island. At 6 AM, the SST is warmer on the west side for both days. The maximum SST difference downstream of the island is 1°C, contributing to the increased heat fluxes to the atmosphere in this region. At 6 PM, the SST range is 27.1 to 27.3°C in the east, increasing to values between 27.6 to 28.1°C in the west. The warm wake area identified downstream coincides with the weakening of the surface currents.

In 2012 (Figure 7), an upper circulation from the east is observed, representing the cSEC, which weakens on the island's west side. At 6 AM, the temperatures are around 26ºC on the island's east side and 27 ºC on the west. At 6 PM, the waters present higher temperatures in the whole domain, as expected, due to the heat storage during the day, also showing 1°C warming on the west side compared to the east.

The results for 2014 (Figure 8) also evidence the warm wake downstream of the island. In this case, the predominant currents are from the east. The warm wake identified in our results is also identified in other islands. The temperature differences between the east and west sides of the island make evident the presence of a warm wake. Caldeira and Marchesiello (2002) also found a warm surface oceanic wake persisting from 6 to 16 June 1999 in the southeastern part of Santa Catalina Island in the Southern California Bight. They found a strong correlation between SST, wind stress, and surface stratification. The authors argue that the warm island wake was probably due to lower turbulent mixing rates associated with the wind sheltering effect.

The SSTs in 2010 were higher than in 2012 and 2014 (Figures 6, 7 and 8). Vale Silva et al. (2018) identified anomalous warming events, with SST anomalies higher than 1 ºC for three consecutive months in the Southern tropical Atlantic. Ibánhez et al. (2017) analyzed this warm

event in the tropical Atlantic, which promoted a significant increase in the CO_2 fugacity of surface waters. This climatological event inverted the CO_2 sink to a source of CO_2 to the atmosphere.
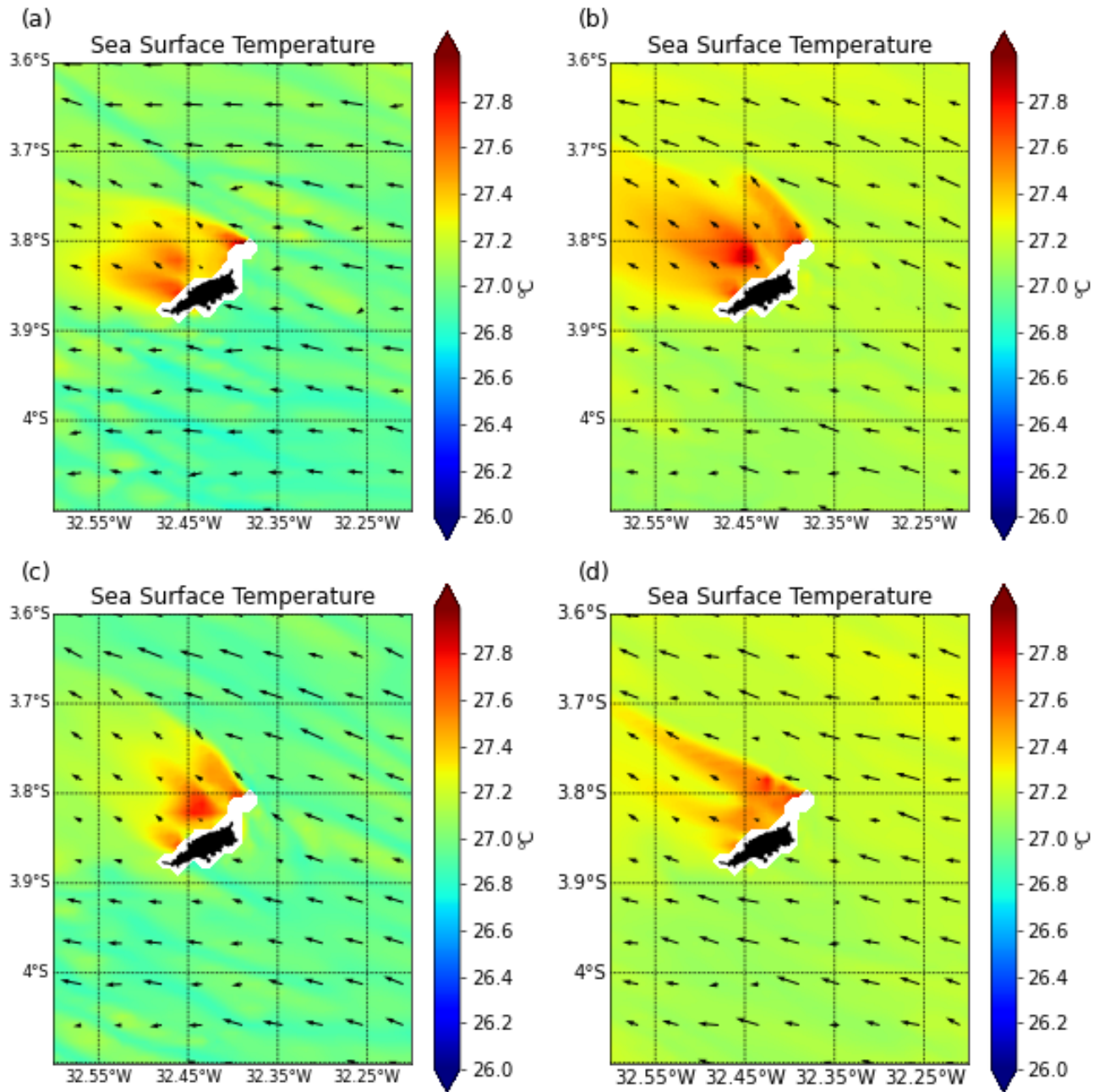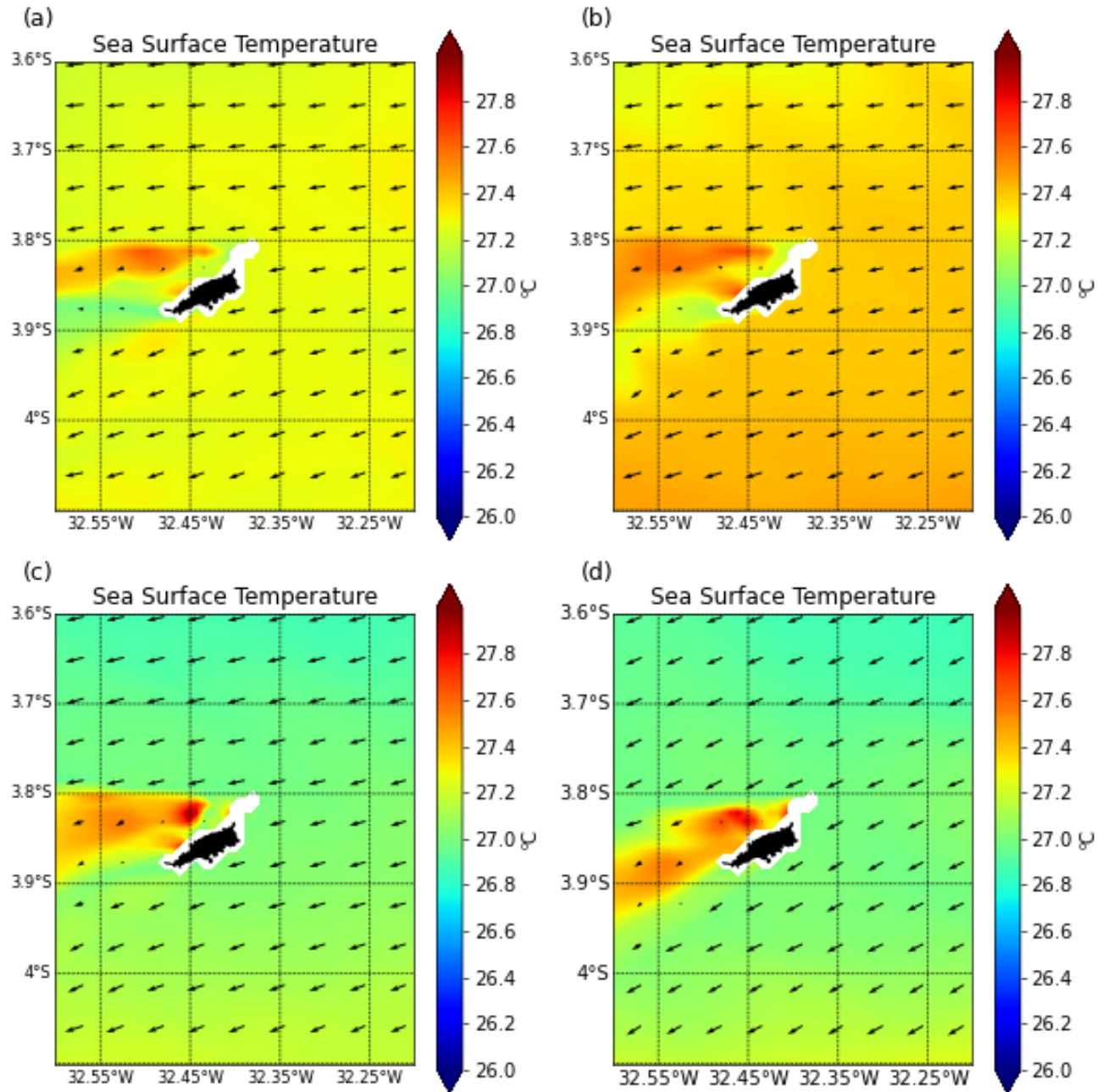

Figure 6. Sea surface temperature and surface currents for the CF2010: (a) 6 AM 01 August 2010, (b) 6 PM 01 August 2010, (c) 6 AM 02 August 2010, (d) 6 PM 02 August 2010.
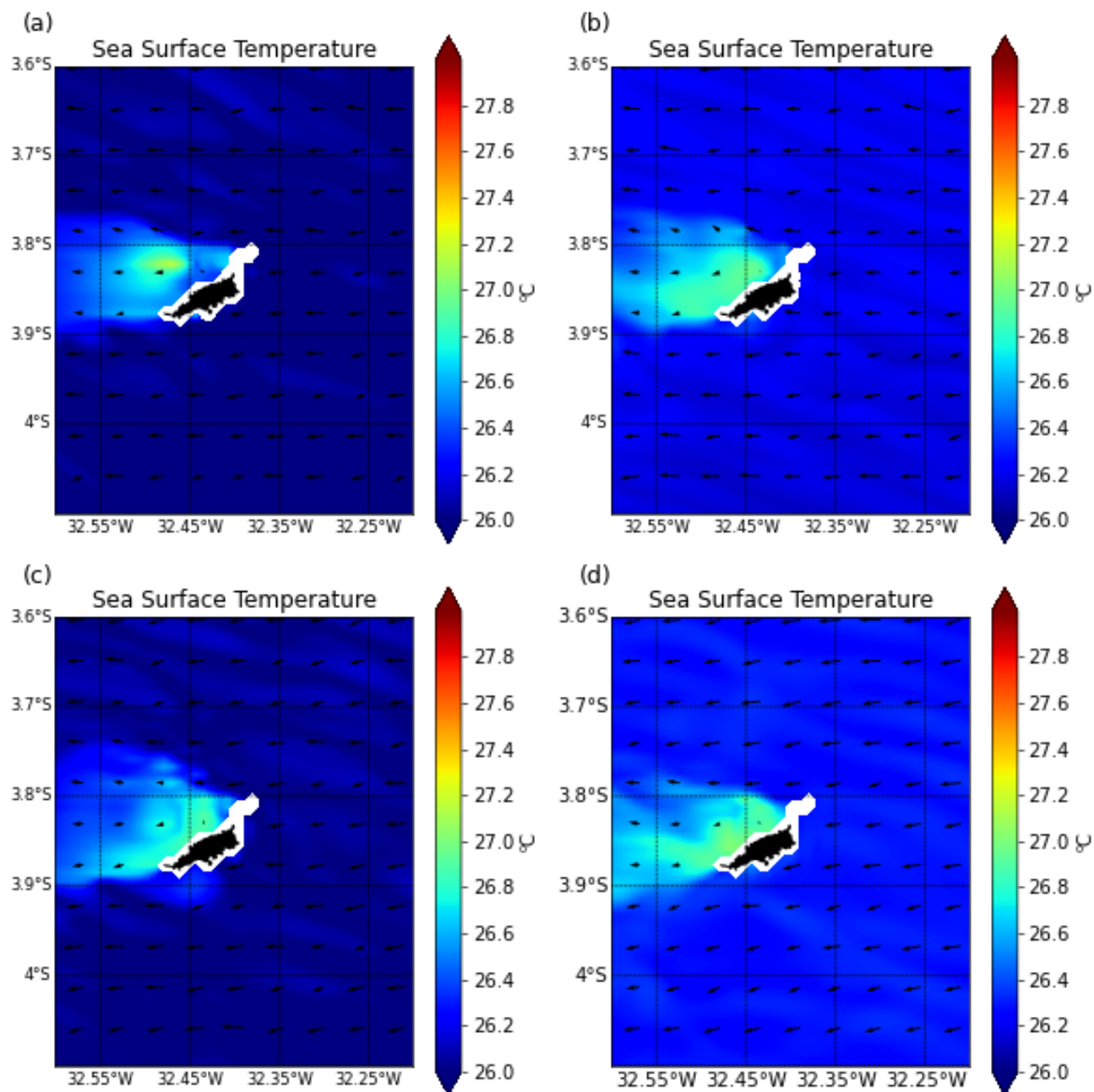
Figure 7. Sea surface temperature and surface currents for the CF2012: (a) 6 AM 24 September 2012, (b) 6 PM 24 September 2012, (c) 6 AM 25 September 2012, (d) 6 PM 25 September 2012.

Figure 8. Sea surface temperature and surface currents for the CF2014: (a) 6 AM 07 July 2014, (b) 6 PM 07 July 2014, (c) 6 AM 08 July 2014, (d) 6 PM 08 July 2014.

The longitudinal cross-section of the ocean-atmosphere coupling (Figure 9) highlights the vertical structure of ocean temperature and currents and the atmospheric response through the winds and air temperature. Our results present an averaged mixed layer depth of 40 m depth. Also, this depth allows us to identify the island's warm wake and its effects on the lower atmosphere. The ocean sections show warmer waters downstream of the island.

In 2010 (Figure 9a,b), there was an intensified downward ocean current component, followed by forced upward motions upstream of the island. This motion favors a mixing and no stratification. After nocturnal ocean heat loss, the atmosphere is warmer at 6 AM, mainly downstream, developing an east-west temperature gradient. As expected, on the west side, due to the presence of the warm wake, a warmer air column expands, about 1 ºC higher than on the east side. The winds follow the island topography, rising upstream and going down downstream. Due to the orographic blocking, the winds are weakened downstream of the island. At 6 PM, however, the longitudinal temperature is more homogeneous. Near the surface, the atmosphere is about 2 °C warmer than the upper ocean, and the winds present the same intensities.

In 2012 (Figure 9c,d), there was an ocean temperature increase (~27 °C) downstream of the island, restricted to the surface. The temperature of the water column has average values of ~26 °C, a pattern quite different from that observed in 2010 when average values were ~28 °C. The atmosphere temperature values near the surface are lower (< 1 °C) than the ocean surface waters. The daily cycle shows the development of a warmer atmosphere at 6 PM. Both ocean and atmospheric averaged temperatures are colder compared to 2012 and 2014.

In 2014 (Figure 9e,f), the ocean currents revealed an anomalous upward component downstream near the island. Colder waters at 20-40m depth are associated with this upward motion. However, these cold waters are not forced enough to emerge at the surface. A subsurface uplift of the thermohaline structure was also identified by Silva et al. (2019) with in situ data. Tchamabi et al. (2017) also identified an uplift through climatological modeling results and in situ data. At 6 AM, downstream of the island, the ocean's warm wake is present in the first 20 m, and the atmosphere air column is warmed over this area. At 6 PM, the warm wake prevails downstream, and the atmosphere is warmed.
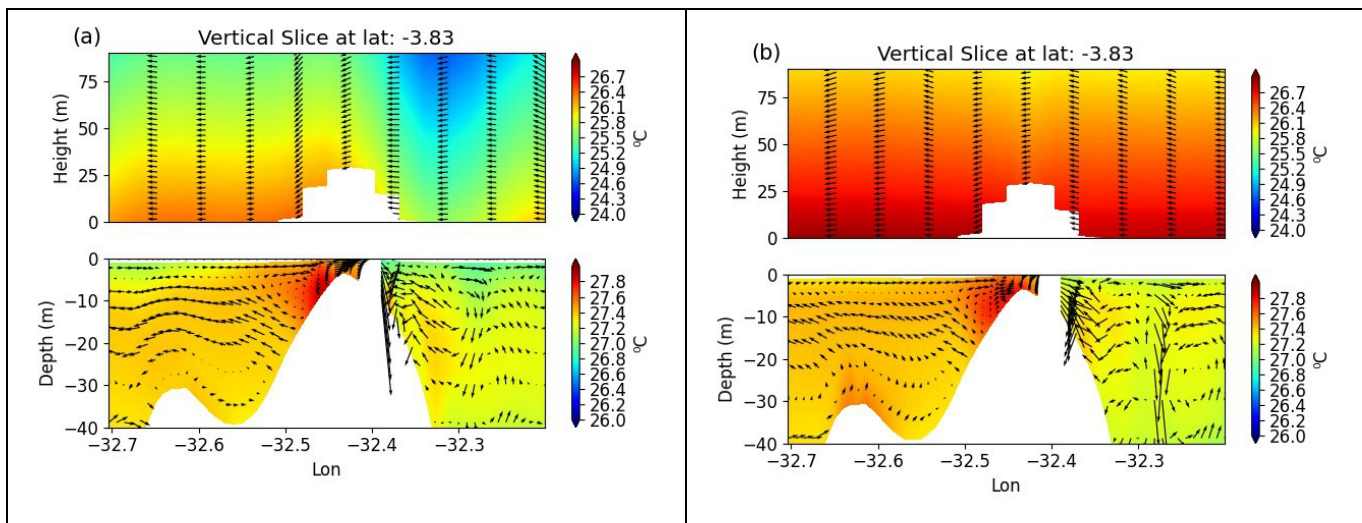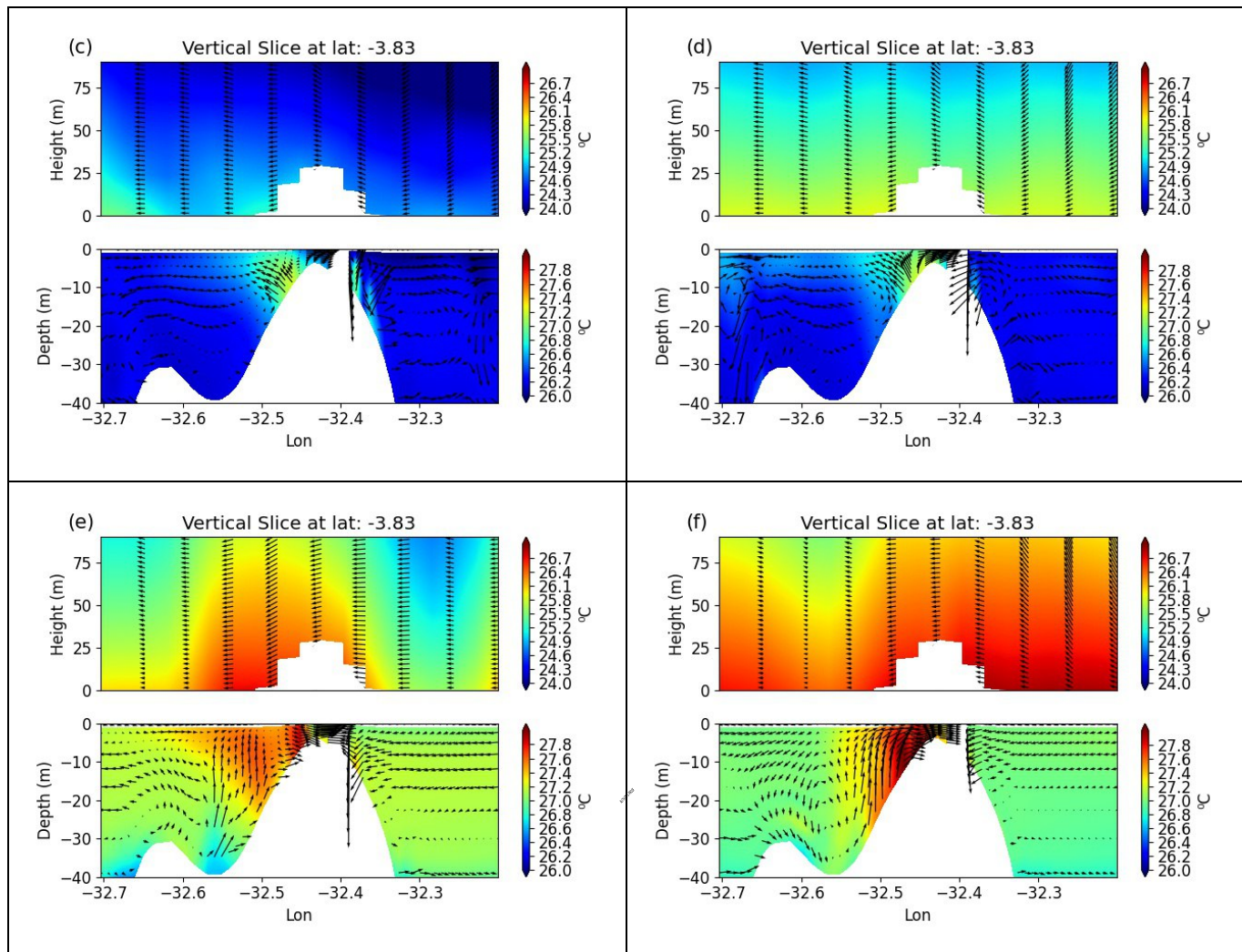
Figure 9. WRF-ROMS sections of ocean temperature and currents and atmosphere temperature and winds, for: (a) 01 August 2010 6 AM and (b) 6 PM, (c) 24 September 2012 6 AM, (d) 24 September 2012 6 PM, (e) 07 July 2014 6 AM and (f) 6 PM.

Air-sea CO$_2$ Fluxes

This section presents the modeled results of seawater CO$_2$ fugacity, calculated with equation 5, and the air-sea CO$_2$ fluxes (FCO$_2$) estimated by equation 2. Among the three cruises, only the CF2012 had measurements of fCO$_2$sw around the FN. Figures 10a,b show the fCO$_2$sw (μatm) and temperature (°C) measurements from CF2012. Figures 10c,d show the modeled fCO$_2$sw and temperature at the same points of the CF2012 cruise. Figures 10e,f show the bias between the modeled and in situ data. The bias maps show that the modeling underestimated (~ -0,3 °C) the observed temperature, except at the west of the island (~ +0,3 °C), where the model temperature is higher than the measurements. The fCO$_2$ bias shows that the model

underestimates the measurements in about -20 mmol m^{-2} d^{-1}. Despite the low-temperature differences, it could contribute to the weaker CO$_2$ fluxes around the island.
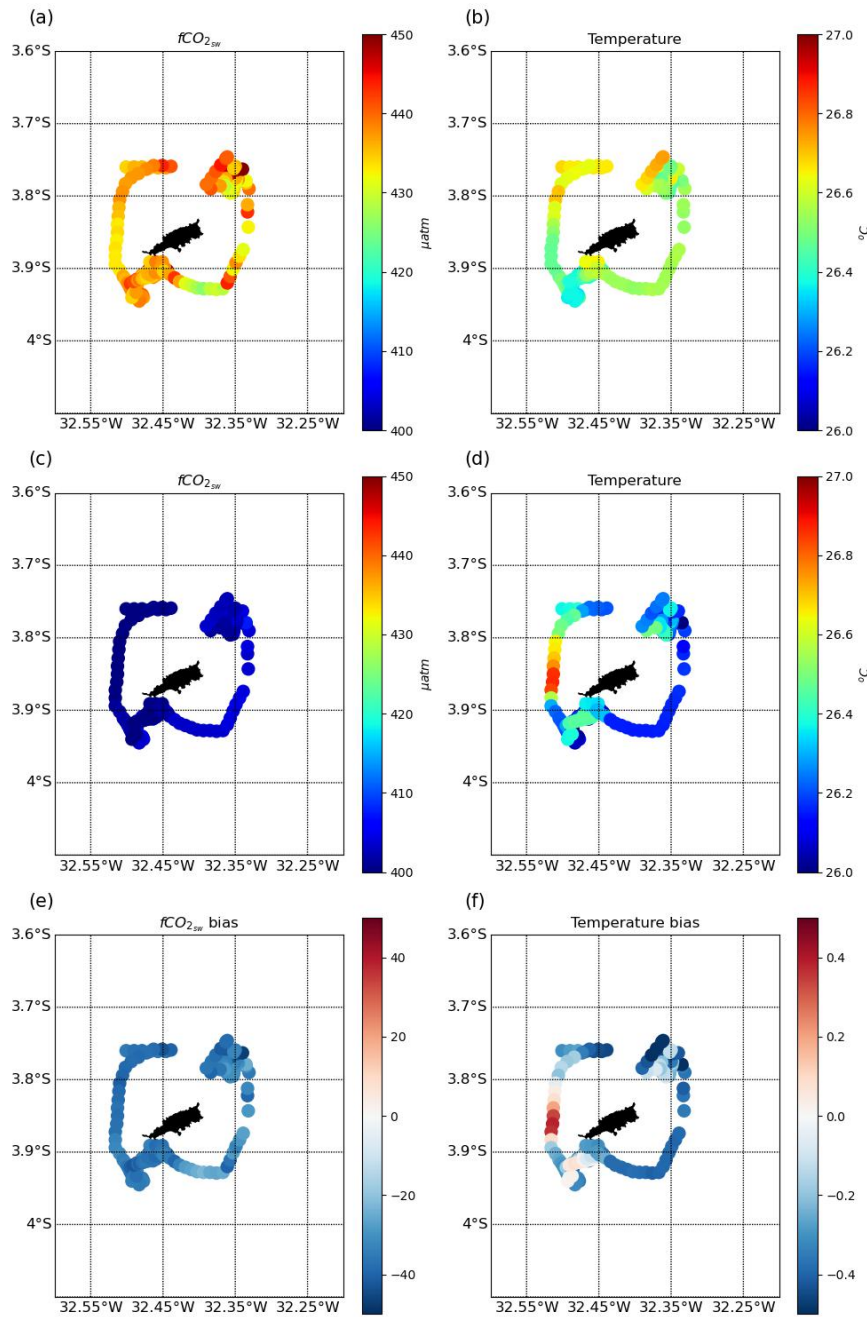
Figure 10. Seawater fCO$_2$ in μatm (a) September 24, 2012, at 6AM, (b) at 6 PM (c) September 25, 2012 at 6AM and (d) 6 PM, (e) fCO$_2$ modeled – observed, (f) temperature modeled - observed.

Figures 11, 12, and 13 show the modeled results of air-sea FCO_2 using the fCO_2sw based on equation 5. The results show only positive FCO_2 and lower values west of the island (Figure 11, Figure 12, and Figure 13).
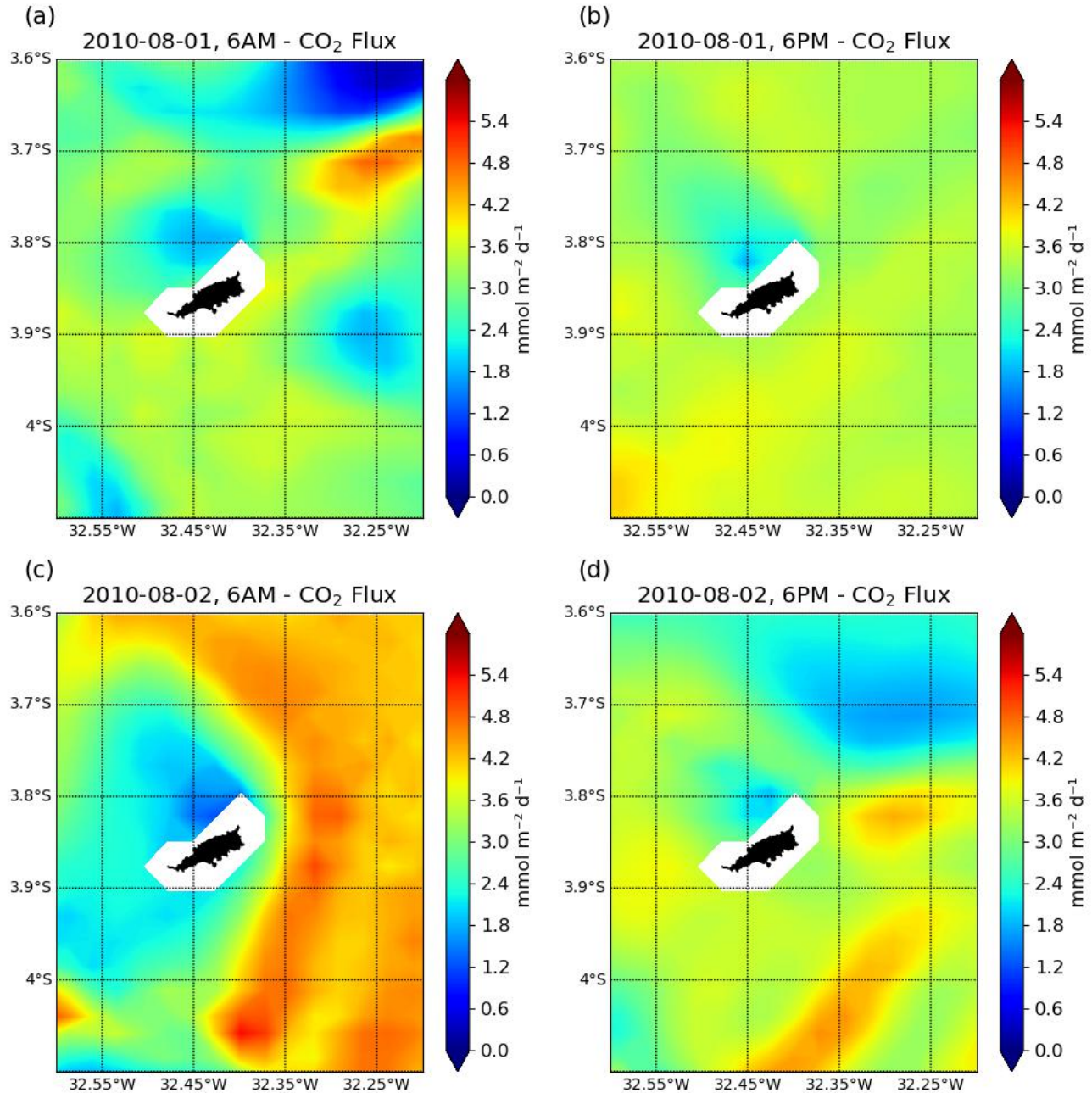

Figure 11. Air-sea FCO_2: (a) August 01, 2010, at 6AM, (b) at 6 PM (c) August 02, 2010 at 6AM and (d) 6 PM.

The results show only positive FCO_2, which is expected for the tropical Atlantic. However, a weakening of the FCO_2 in the Northwest of the island is evident, mainly in 2010 and 2012. According to Figure 9c, during the CF2012, the atmosphere was colder than the ocean, and Figure 7 shows the weakening of surface currents at the Northwest of the island. This weakening in the surface circulation reduces the mixing of the water column and increases the SST. The increased SST associated with a colder atmosphere can contribute to the positive FCO_2 in the whole domain. Takahashi et al. (1993) reported a thermodynamic effect with an increase of 4% in seawater fCO_2 for a 1°C increase if warming is the only process. This fCO_2 increase might be observed on the CO_2 flux if no other changes occur. However, for 2010, at 6 AM (Figure 9a), the surface ocean is about 0.5°C warmer than the lower atmosphere, but both present the same temperature at 6 PM (Figure 9b). The same occurred in 2014, with no significant vertical temperature gradients between the ocean and atmosphere. The vertical gradient absence occurs mainly downstream of the island due to the temperature of the warm wake reaching similar temperatures as in the atmosphere. The ocean heat loss to the atmosphere could equilibrate the temperatures and induce the reduced FCO_2 at the Northwest of the island.
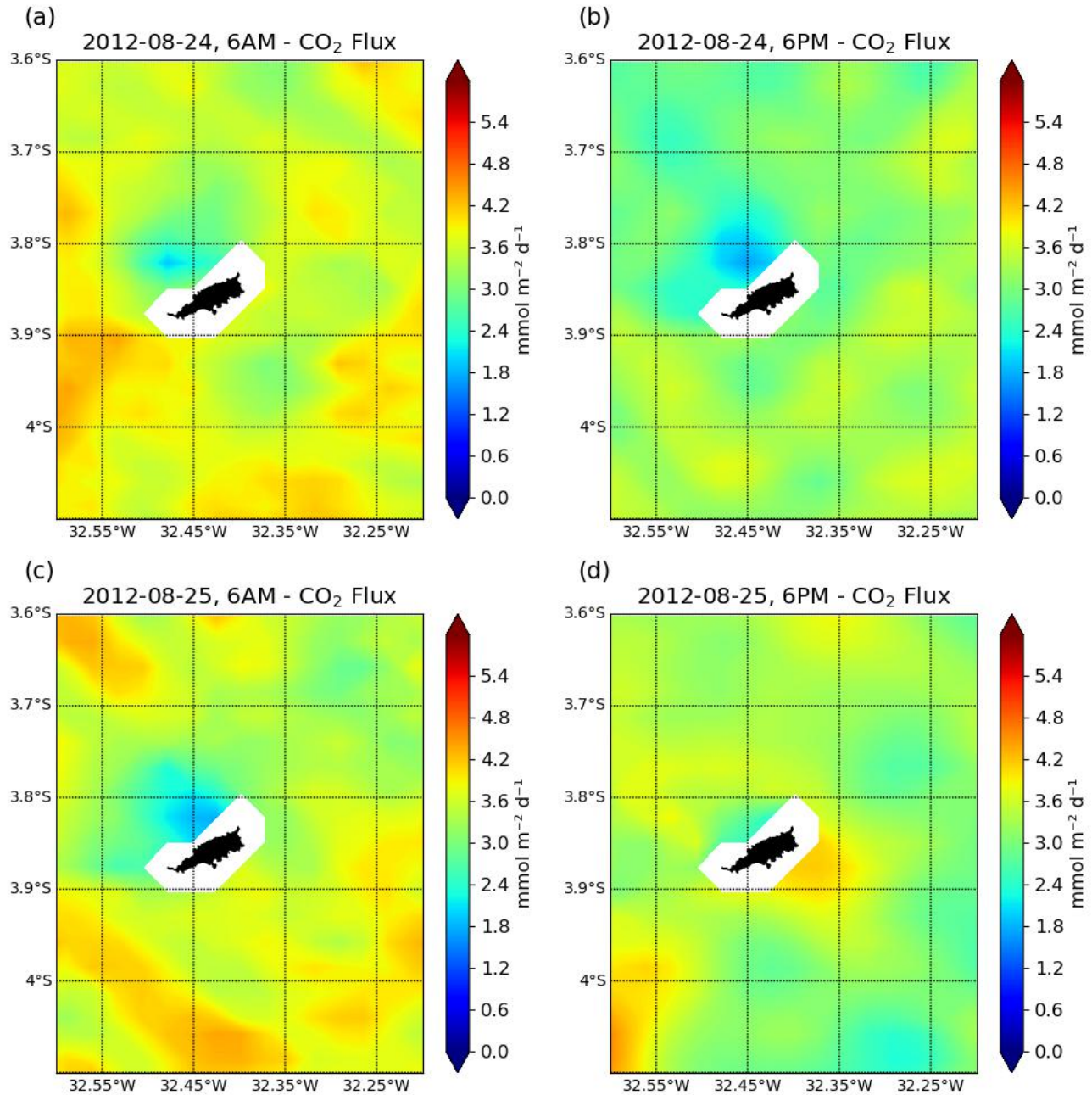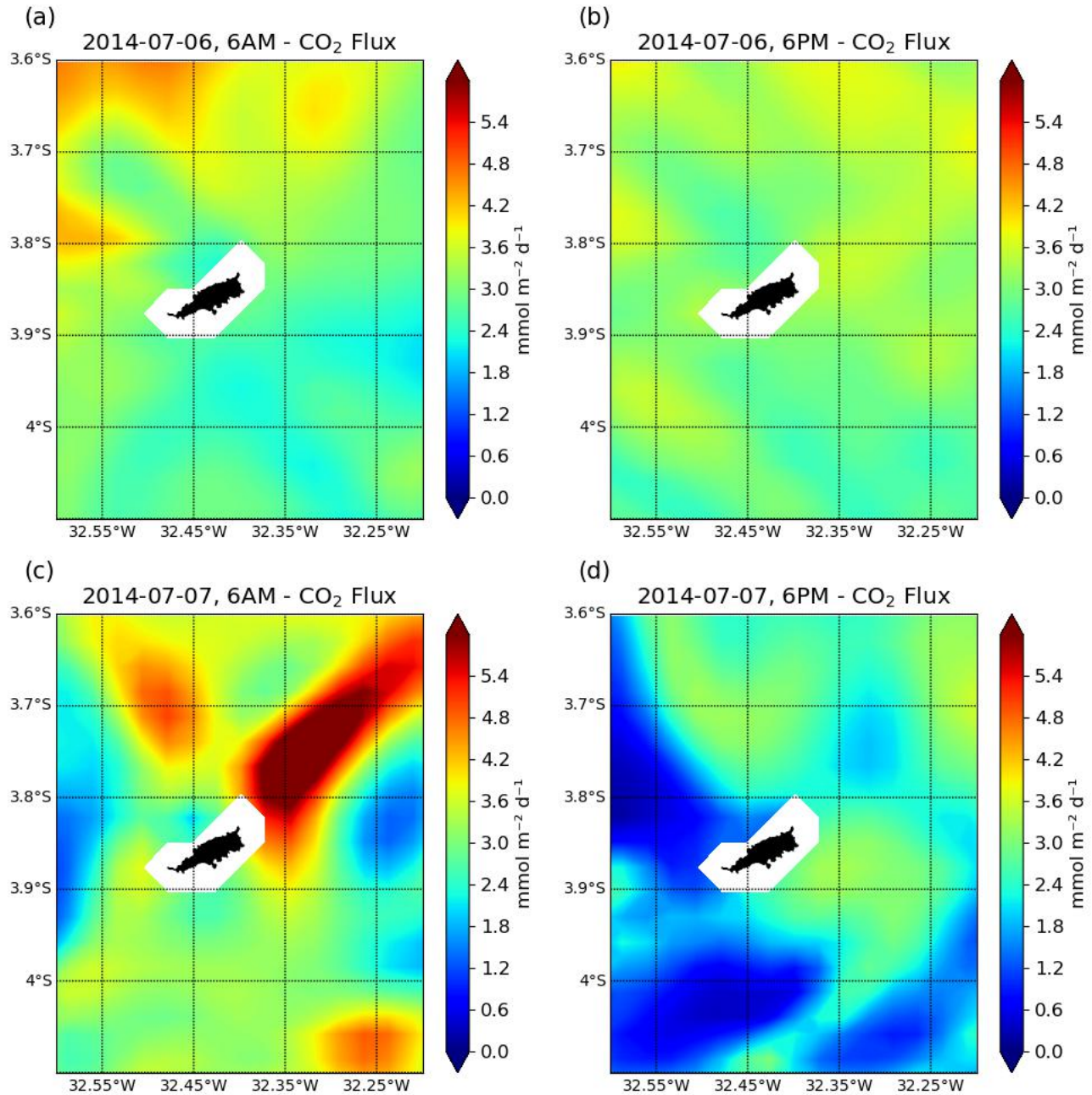
Figure 12. Air-sea FCO$_2$: (a) September 24, 2012 at 6AM, (b) at 6 PM (c) September 25, 2012 at 6AM and (d) 6 PM.

Figure 13. Air-sea FCO_2: (a) July 06, 2014, at 6AM, (b) at 6 PM (c) July 07, 2014 at 6AM and (d) 6 PM.

The FCO_2 shows different spatial variability for 2010, 2012, and 2014 (Figure 11, Figure 12, and Figure 13). There was a high amplitude in the FCO_2 values in 2010, ranging from 0 to 6.6 mmol m^{-2} d^{-1} (Figure 11). At the Northwest of the island, there is a reduced FCO_2 area of about 2mmol m^{-2} s^{-1} compared to the whole domain. This Northwest low FCO_2 area coincides with the island's warm wake. The reduced FCO_2 could be associated with warmer atmosphere

temperatures than in the ocean (Figure 10a, b). In fact, 2010 was an anomalous warmer year, as evidenced by Vale Silva et al. (2018).

In 2012 (Figure 12), the CO_2 fluxes ranged from 2.4 to 5.4 mmol m^{-2} d^{-1}. The low FCO_2 Northwestern area is weaker compared with 2010. This year, the average temperatures in both ocean and atmosphere were colder, evidencing a weaker warm wake effect compared to 2012 and 2014.

2014, the fluxes presented substantial spatial differences between July 6 and 7. For day 6, there is a quasi-homogeneous spatial FCO_2 distribution. On the morning of day 7, there is a strong source of FCO_2 Northeast of the island (Figure 13a). In the afternoon (Figure 13b), there is a reduction in the FCO_2 flux around the whole west ocean region. The ocean-atmosphere temperature gradient on July 7 was weak. According to the results of air-sea temperature (Figure 9) for July 7, the difference between the atmosphere and ocean decreased.

Conclusion

This work investigated thermodynamic conditions and air-sea CO_2 fluxes based on in-situ and ocean-atmosphere coupled modeling data in the Fernando de Noronha Island region. The main challenge was to simulate the realistic thermodynamic conditions around the island using a coupled model. The validation analyses performed with the Taylor diagram showed that the ocean-atmospheric modeling results agree well with three oceanographic cruises around the island. The temperature and salinity profiles of the model were remarkably close to the profiles obtained in the three oceanographic cruises, as well as the modeled winds that also agree with the in situ 10m wind speed and direction values.

The physical barrier of the island constrains the flow circulating it, which induces instabilities and other related processes upstream and downstream. Hence, the island modifies the sea surface temperature and currents. On the island's west side, the ocean currents are weakened due to the physical barrier, and the SST increases, diverging from adjacent waters. In 2010, there was damming on the island's northwest side, and in 2014 the same occurred in the island's western region. The island effect is also observed when analyzing the vertical section. In 2010, the air temperature was higher than in 2014. In the atmosphere, the wind contours the upper terrain of the island. In the ocean, a temperature gradient and some turbulence occur on the west side of the island.

The CO_2 fluxes were estimated using physical variables from the ocean-atmospheric modeling results. The FCO_2 in 2010 and 2012 showed higher values of CO_2 released into the

atmosphere than in 2014. Our results show that in 2010, the water column temperature was warmer with ~27°C. Also, previous works found that SST anomalies in 2010 were higher than 1°C in this region and persisted for at least three months (Vale Silva et al., 2018). 2012 presented colder waters than in 2010, ~26°C, and a reduced gradient between ocean and atmosphere temperatures, which can decrease the air-sea partial pressure CO_2 and reduce the fluxes. The modeled fCO_2 underestimated the measurements, but overall, the ocean was a source of CO_2 for the atmosphere during the three cruise periods. This study presented an initial investigation using a coupled ocean-atmosphere model for Fernando de Noronha Island. The following steps involve activating the biogeochemical module to the coupled ocean-atmosphere model. This information will allow a more accurate estimate of FCO_2 at the ocean-atmosphere interface around the island of Fernando de Noronha.

Acknowledgments

References

Amante, C., & Eakins, B. (2009). ETOPO1 1 Arc-Minute Global Relief Model: procedures, data sources and analysis. NOAA Technical Memorandum NES-DIS NGDC, 24. DOI: 10.7289/V5C8276

Araujo, M., Noriega, C., Medeiros, C., Lefèvre, N., Ibánhez, J. S. P., Flores Montes, M., Santos, M. d. L. (2019). On the variability in the CO_2 system and water productivity in the western tropical Atlantic off North and North-east Brazil. Journal of Marine Systems, 189 (September 2018), 62–77. DOI: 10.1016/j.jmarsys.2018.09.008

Araujo M., Cintra M. (2009). Modelagem matemática da circulação oceânica na região equatorial. In Viana D. L. [et al.,] (Orgs.) O arquipélago São Pedro e São Paulo: 10 anos de Estação científica/ Brasília, DF: SECIRM. pp. 106–113.

Arístegui, J., Tett, P., Hernández-Guerra, A., Basterretxea, G., Montero, M. F., Wild, K., Barton, E. D. (1997). The influence of island-generated eddies on chlorophyll distribution: A study of mesoscale variation around Gran Canaria. Deep-Sea Research Part I: Oceanographic Research Papers, 44 (1), 71–96. DOI: 10.1016/S0967-0637(96)00093-3

Bakker, D. C. E., Nielsdóttir, M. C., Morris, P. J., Venables, H. J., & Watson, A. J. (2007). The island mass effect and biological carbon uptake for the sub- Antarctic Crozet Archipelago. Deep-Sea Research Part II: Topical Studies in Oceanography, 54 (18-20), 2174–2190. DOI: 10.1016/j.dsr2.2007.06.009

Bates, N. R., Mathis, J. T., & Jeffries, M. A. (2011). Air-sea CO_2 fluxes on the Bering Sea shelf. Biogeosciences, 8 (5), 1237–1253. DOI: 10.5194/bg-8-1237 -2011

Bertini, L. and Braga, E. (2022). The Contribution of Nutrients and Water Properties to the Carbonate System in Three Particular Areas of the Tropical Atlantic (NE-BRAZIL). Journal of Geoscience and Environment Protection, 10, 135-161. DOI: 10.4236/gep.2022.102009.

Brandão, C. dos S., Malta, A., & Schiavetti, A. (2017). Temporal assessment of the management effectiveness of reef environments: The role of marine protected areas in Brazil. Ocean and Coastal Management, 142, 111–121. DOI: 10.1016/j.ocecoaman.2017.03.015

Burgers, T. M., Miller, L. A., Thomas, H., Else, B. G. T., Gosselin, M., & Papakyriakou, T. (2017). Surface Water pCO_2 Variations and Sea-Air CO_2 Fluxes During Summer in the Eastern Canadian Arctic. Journal of Geophysical Research: Oceans, 122 (12), 9663–9678. DOI: 10.1002/2017JC013250

Caldeira, R. M. A., & Marchesiello, P. (2002). Ocean response to wind sheltering in the Southern California Bight. Geophysical Research Letters, 29(13), 1635–1639. DOI: 10.1029/2001GL014563

Caldeira, R. M. A., Groom, S., Miller, P., Pilgrim, D., & Nezlin, N. P. (2002). Sea-surface signatures of the island mass effect phenomena around Madeira Island, Northeast Atlantic. Remote Sensing of Environment, 80(2), 336–360. DOI: 10.1016/S0034-4257(01)00316-9

Caldeira, R. M., Marchesiello, P., Nezlin, N. P., DiGiacomo, P. M., & McWilliams, J. C. (2005). Island wakes in the Southern California Bight. Journal of Geophysical Research: Oceans, 110 (11), 1–20. DOI: 10.1029/2004JC002675

Caldeira, R.M.A., Tomé, R. (2013). Wake Response to an Ocean-Feedback Mechanism: Madeira Island Case Study. Boundary-Layer Meteorol 148, 419–436. DOI: 10.1007/s10546-013-9817-y

Chaves, T. B. C., Mafalda JR., P., Santos, C., de Souza, C. S., Moura, G., Sampaio, J., Feitosa, F. A. d. N. (2006). Biomassa planctônica e hidrografia na zona econômica exclusiva do Nordeste do Brasil. Tropical Oceanography, 34 (1), 12–30.

Costa da Silva A, Chaigneau A, Dossa AN, Eldin G, Araujo M and Bertrand A (2021). Surface Circulation and Vertical Structure of Upper Ocean Variability Around Fernando de Noronha Archipelago and Rocas Atoll During Spring 2015 and Fall 2017. Front. Mar. Sci. 8:598101. DOI: 10.3389/fmars.2021.598101

Currie, K. I., Macaskill, B., Reid, M. R., & Law, C. S. (2011). Processes governing the carbon chemistry during the SAGE experiment. Deep-Sea Research Part II: Topical Studies in Oceanography, 58 (6), 851–860. DOI: 10.1016/j.dsr2.2010.10.023

Dai, M., Lu, Z., Zhai, W., Chen, B., Cao, Z., Zhou, K., Chenc, C.-T. A. (2009). Diurnal variations of surface seawater pCO_2 in contrasting coastal environments. Limnology and Oceanography, 54 (3), 735–745. DOI: 10.4319/lo.2009.54.3.0735

Drupp, P., de Carlo, E. H., Mackenzie, F. T., Bienfang, P., & Sabine, C. L. (2011). Nutrient Inputs, Phytoplankton Response, and CO_2 Variations in a Semi-Enclosed Subtropical Embayment, Kaneohe Bay, Hawaii. Aquatic Geo-chemistry, 17 (4), 473–498. DOI: 10.1007/s10498-010-9115-y

Dumousseaud, C., Achterberg, E. P., Tyrrell, T., Charalampopoulou, A., Schuster, U., Hartman, M., & Hydes, D. J. (2010). Contrasting effects of temperature and winter mixing on the seasonal and inter-annual variability of the carbonate system in the Northeast Atlantic Ocean. Biogeosciences, 7 (5), 1481–1492. DOI: 10.5194/bg-7-1481-2010

Ekau, W., & Knoppers, B. (1999). An introduction to the pelagic system of the North-East and East Brazilian shelf. Archive of Fishery and Marine Research, 47 (2/3), 5–24. DOI: 0944-1921/99/47/2/3-5/12.00$/0

Esters, L., Landwehr, S., Sutherland, G., Bell, T. G., Christensen, K. H., Saltzman, E. S., Ward, B. (2017). Parameterizing air-sea gas transfer velocity with dissipation. Journal of Geophysical Research: Oceans, 122 (4), 3041– 056. DOI: 10.1002/2016JC012088

Evans, W., Hales, B., Strutton, P. G., & Ianson, D. (2012). Sea-air CO_2 fluxes in the western Canadian coastal ocean. Progress in Oceanography, 101 (1), 78– 91. DOI: 10.1016/j.pocean.2012.01.003

Fransson, S., Woolf, D. K., Jeffrey, C. D., & Robinson, I. S. (2008). Calculating long-term global air-sea flux of carbon dioxide using scatterometer, passive microwave, and model reanalysis wind data. Journal of Geophysical Research: Oceans, 113 (9), 14. DOI: 10.1029/2005JC003376

Friedman, J. R., Shadwick, E. H., Friedrichs, M. A. M., Najjar, R. G., De Meo, O. A., Da, F., & Smith, J. L. (2020). Seasonal Variability of the CO_2 System in a Large Coastal Plain Estuary. Journal of Geophysical Research: Oceans, 125 (1). DOI: 10.1029/2019JC015609

Garla, R. C., Chapman, D. D., Shivji, M. S., Wetherbee, B. M., & Amorim, A. F. (2006). Habitat of juvenile Caribbean reef sharks, Carcharhinus perezi, at two oceanic insular marine protected areas in the southwestern Atlantic Ocean: Fernando de Noronha Archipelago and Atol das Rocas, Brazil. Fisheries Research, 81(2–3), 236–241. DOI: 10.1016/j.fishres.2006.07.003

Garzke, J., Hansen, T., Ismar, S. M. H., & Sommer, U. (2016). Combined effects of ocean warming and acidification on copepod abundance, body size and fatty acid content. PLoS ONE, 11 (5). DOI: 10.1371/journal.pone.0155952

Gove, J. M., McManus, M. A., Neuheimer, A. B., Polovina, J. J., Drazen, J. C., Smith, C. R., et al. (2016). Near island biological hotspots in barren ocean basins. Nature Communications, 7(1), 10581. DOI: 10.1038/ncomms10581

Han, G., Dong, C., Li, J., Yang, J., Wang, Q., Liu, Y., & Sommeria, J. (2019). SST anomalies in the Mozambique Channel using remote sensing and numerical modeling data. Remote Sensing, 11(9). DOI: 10.3390/rs11091112

Humphreys, M. P., Daniels, C. J., Wolf-Gladrow, D. A., Tyrrell, T., & Achterberg, E. P. (2018). On the influence of marine biogeochemical processes over CO_2 exchange between the atmosphere and ocean. Marine Chemistry, 199(June 2017), 1–11. DOI: 10.1016/j.marchem.2017.12.006

Ibánhez, J. S. P., Flores, M., & Lefèvre, N. (2017). Collapse of the tropical and subtropical North Atlantic CO_2 sink in boreal spring of 2010. Scientific Reports, 7(July 2016), 1–9. DOI: 10.1038/srep41694

Jacob, R., Larson, J., & Ong, E. (2005). M × N Communication and Parallel Interpolation in Community Climate System Model Version 3 Using the Model Coupling Toolkit. IJHPCA, 19, 293–307. DOI: 10.1177/1094342005056116

Larson, J., Jacob, R., & Ong, E. (2005). The Model Coupling Toolkit: A New Fortran90 Toolkit for Building Multiphysics Parallel Coupled Models. The International Journal of High-Performance Computing Applications, 19 (3), 277–292. DOI: 10.1177/1094342005056115

Lefèvre, N., Diverrés, D., & Gallois, F. (2010). Origin of CO_2 undersaturation in the western tropical Atlantic. Tellus, Series B: Chemical and Physical Meteorology, 62 (5), 595–607. DOI: 10.1111/j.1600-0889.2010.00475.x

Lefèvre, N., Urbano, D. F., Gallois, F., & Diverrè, D. (2014). Impact of physical processes on the seasonal distribution of the fugacity of CO_2 in the western tropical Atlantic. Journal of Geophysical Research: Oceans, 119 (2), 1383–1419. DOI: 10.1002/2013JC008979.Received

Leite, T. S., Haimovici, M., Mather, J., & Oliveira, J. E. L. (2009). Habitat, distribution, and abundance of the commercial octopus (Octopus insularis) in a tropical oceanic island, Brazil: Information for management of an artisanal fishery inside a marine protected area. Fisheries Research, 98(1–3), 85–91. DOI: 10.1016/j.fishres.2009.04.001

Lencina-Avila, J. M., Ito, R. G., Garcia, C. A. E., & Tavano, V. M. (2016). Sea-air carbon dioxide fluxes along 35°S in the South Atlantic Ocean. Deep-Sea Research Part I: Oceanographic Research Papers, 115, 175–187. DOI: 10.1016/j.dsr.2016.06.004

Li, H., Ilyina, T., Müller, W. A., & Landschützer, P. (2019). Predicting the variable ocean carbon sink. Science Advances, 5 (4). DOI: 10.1126/sciadv.aav6471

Lumpkin, R., & Garzoli, S. L. (2005). Near-surface circulation in the Tropical Atlantic Ocean. Deep-Sea Research Part I: Oceanographic Research Papers, 52(3), 495–518. DOI: 10.1016/j.dsr.2004.09.001

Mohr, L.V.; Castro, J.W.A.; Costa, P.M.S., and Alves, R.J.V. (2009). Ilhas oceânicas brasileiras: da pesquisa ao manejo. Vol. II, MMA Secretaria de Biodiversidade e Floresta, Brasília, Brasil, 496p. (In Portuguese)

Padin, X. A., Vázquez-Rodríguez, M., Castaño, M., Velo, A., Alonso-Pérez, F., Gago, J., Perez, F. F. (2010). Air-Sea CO_2 fluxes in the Atlantic as measured during boreal spring and autumn. Biogeosciences, 7 (5), 1587–606. DOI: 10.5194/bg-7-1587-2010

Pullen, J., Caldeira, R., Doyle, J. D., May, P., Tomé, R. (2017): Modeling the Air-Sea Feedback System of Madeira Island. Journal of Advances in Modeling Earth Systems, 9(3), 1641-1664

Sangrà, P., Auladell, M., Marrero-Díaz, A., Pelegrí, J. L., Fraile-Nuez, E., Rodríguez-Santana, A., Hernández-Guerra, A. (2007). On the nature of oceanic eddies shed by the Island of Gran

Canaria. Deep-Sea Research Part I: Oceanographic Research Papers, 54(5), 687–709. DOI: 10.1016/j.dsr.2007.02.004

Schuster, U., Watson, A. J., Bates, N. R., Corbiere, A., Gonzalez-Davila, M., Metzl, N., . . . Santana-Casiano, M. (2009a). Trends in North Atlantic sea-surface fCO$_2$ from 1990 to 2006. Deep-Sea Research Part II: Topical Studies in Oceanography, 56 (8-10), 620–629. DOI: 10.1016/j.dsr2.2008.12.011

Shchepetkin, A. F., & McWilliams, J. C. (2005). The regional oceanic modeling system (ROMS): a split-explicit, free-surface, topography-following-coordinate oceanic model. Ocean Modelling, 9 (4), 347–404. DOI: 10.1016/j.ocemod.2004.08.002

Silva, B. J., Gaspar, F. L., Tyaquiçã, P., Lefèvre, N., & Flores Montes, M. J. (2019). Carbon chemistry variability around a tropical archipelago. Marine and Freshwater Research, 70 (6), 767–780.

Skamarock, W. C., Klemp, J. B., Dudhia, J., Gill, D. O., Barker, D. M., Wang, W., & Powers, J. G. (2005). A description of the advanced research WRF version 2. NCAR TECHNICAL NOTE (June), 100.

Sweeney, C., Gloor, E., Jacobson, A. R., Key, R. M., McKinley, G., Sarmiento, J. L., & Wanninkhof, R. (2007). Constraining global air-sea gas exchange for CO 2 with recent bomb 14 C measurements. Global Biogeochemical Cycles, 21 (2), 10. DOI: 10.1029/2006GB002784

Takahashi, T., Olafsson, J., Goddard, J. G., Chipman, D. W., and Sutherland, S. C. (1993). Seasonal variation of CO$_2$ and nutrients in the high-latitude surface oceans: a comparative study. Global Biogeochem. Cycles 7, 843–878. doi: 10.1029/93gb02263

Taylor, K. E. (2001). Summarizing multiple aspects of model performance in a single diagram. Journal ofGeophysical Research, 106, 7183–7192. DOI: 10.1029/2000JD900719

Tchamabi, C. C., Araujo, M., Silva, M., & Bourlès, B. (2017). A study of the Brazilian Fernando de Noronha Island and Rocas atoll wakes in the tropical Atlantic. Ocean Modelling, 111, 9–18. DOI: 10.1016/j.ocemod.2016.12.009

Torres, R., Artioli, Y., Kitidis, V., Ciavatta, S., Ruiz-Villarreal, M., Shutler, J., … Tilstone, G. H. (2020). Sensitivity of modeled CO$_2$ air-sea flux in a coastal environment to surface temperature gradients, surfactants, and satellite data assimilation. Remote Sensing, 12(12). DOI: 10.3390/RS12122038

Tozer, B, Sandwell, D. T., Smith, W. H. F., Olson, C., Beale, J. R., & Wessel, P. (2019). Global bathymetry and topography at 15 arc sec: SRTM15+. Earth and Space Science, 6, 1847–1864. https://doi.org/10.1029/2019EA000658

Vale Silva, T., D. Veleda, M. Araujo, and P. Tyaquiçã (2018). Ocean–Atmosphere Feedback during Extreme Rainfall Events in Eastern Northeast Brazil. J. Appl. Meteor. Climatol., 57, 1211–1229, https://doi.org/10.1175/JAMC-D-17-0232.1.

Vargas, G., Lucena-Frédou, F., Habasque, J., Lebourges-Dhaussy, A., Roudaut, G., & Bertrand, A. (2018). A new multifrequency acoustic method for the discrimination of biotic components in pelagic ecosystems: Application in a high diversity tropical ecosystem off Northeast Brazil. In 2017 IEEE/OES Acoustics in Underwater Geosciences Symposium, RIO Acoustics 2017 (Vol. 2018-January, pp. 1–8). Institute of Electrical and Electronics Engineers Inc. DOI: 10.1109/RIOAcoustics.2017.8349719

Wallcraft, A., Metzger, E., & Carroll, S. (2009). Software Design Description for the HYbrid Coordinate Ocean Model (HYCOM), Version 2.2., 149.

Ware, J. R., Smith, S. V., & Reaka-Kudla, M. L. (1992). Coral reefs: sources or sinks of atmospheric CO_2? Coral Reefs, 11 (3), 127–130. DOI: 10.1007/ BF00255465

Warner, J. C., Armstrong, B., He, R., & Zambon, J. B. (2010). Development of a Coupled Ocean–Atmosphere–Wave–Sediment Transport (COAWST) Modeling System. Ocean Modelling, 35 (3), 230–244. DOI: 10.1016/j.ocemod.2010.07.010

Warner, J. C., Sherwood, C. R., Arango, H. G., & Signell, R. P. (2005). Performance of four turbulence closure models implemented using a generic length scale method. Ocean Modelling, 8 (1), 81–113. DOI: 10.1016/j.ocemod.2003.12.003

Weiss, R. F. (1974). Carbon dioxide in water and seawater: the solubility of a non-ideal gas. Marine Chemistry7, 2 (3), 203–215. DOI: 10.5194/bg-13-841-2016

Wilkin, J. L., Arango, H. G., Haidvogel, D. B., Lichtenwalner, C. S., Glenn, S. M., & Hedström, K. S. (2005). A regional ocean modeling system for the Long-term Ecosystem Observatory. Journal of Geophysical Research: Oceans, 110 (6), 1–13. DOI: 10.1029/2003JC002218

Yan, H. Q., Yu, K. F., Shi, Q., Tan, Y. H., Zhang, H. L., Zhao, M. X., . . . Wang, P. X. (2011). Coral reef ecosystems in the South China Sea as a source of atmospheric CO 2 in summer. Chinese Science Bulletin, 56 (7), 676–684. DOI: 10.1007/s11434-011-4372-8

Zhai, W.-D., Dai, M.-H., Chen, B.-S., Guo, X.-H., Li, Q., Shang, S.-L., Zhang, C.-Y., Cai, W.-J., and Wang, D.-X.: Seasonal variations of sea–air CO_2 fluxes in the largest tropical marginal

sea (South China Sea) based on multiple-year underway measurements, Biogeosciences, 10, 7775–7791, DOI: 10.5194/bg-10-7775-2013, 2013.